Research Square

Preprints are preliminary reports that have not undergone peer review.
They should not be considered conclusive, used to inform clinical practice,
or referenced by the media as validated information.

Acute phosphate-salt exposure and expression of iron- and heme-related genes in HepaRG cells

Takeshi Honda
Kurume University School of Medicine
Tatsuya Sakaguchi
Nagasaki University
Yuka Kondo
Kurume University School of Medicine
Yuma Yabune
Kurume University School of Medicine
Yoshihiro Motomiya
Suiyukai Clinic
Yuichiro Higashimoto
higashiy@med.kurume-u.ac.jp

Kurume University School of Medicine

Research Article

Keywords: phosphate, HepaRG, hemojuvelin, transferrin, hemopexin, iron metabolism

Posted Date: November 9th, 2026

DOI: https://doi.org/10.21203/rs.3.rs-11461562/v1

License: This work is licensed under a Creative Commons Attribution 4.0 International License.
Read Full License

Additional Declarations: No competing interests reported.

Abstract

Background

Hepatic iron regulation involves iron transport, heme handling, and hepcidin regulation. We examined whether acute phosphate-salt exposure alters related transcripts in HepaRG cells. An earlier report on these data addressed albumin, HNF4A, and ERK activation.

Methods and Results

We reanalyzed a previously generated RNA sequencing (RNA-seq) dataset of HepaRG cells treated for 24 h with vehicle or phosphate (5.0 mM total; three samples per condition). Selected transcripts were measured by quantitative PCR (qPCR) in four to six independent cultures per target and compared by paired log-scale tests with Holm correction across nine targets. RNA-seq showed lower expression of hemojuvelin (HJV), transferrin (TF), hemopexin (HPX), and aminolevulinate dehydratase (ALAD) at a false discovery rate (FDR) below 0.05. A limma-voom reanalysis gave concordant results. By qPCR, HJV expression was lower in all six cultures (geometric mean phosphate-to-vehicle ratio 0.268; 95% confidence interval [CI] 0.157–0.458; Holm-adjusted p = 0.013). The ratios for TF, HPX, matriptase-2 (TMPRSS6), transferrin receptor 2 (TFR2), and ALAD were 0.396, 0.516, 0.425, 0.460, and 0.422, respectively, none significant after Holm adjustment. Estimates for ferritin heavy chain 1 (FTH1) and heme oxygenase 1 (HMOX1) were close to unity, and biliverdin reductase A (BLVRA) showed no clear change. Hepcidin (HAMP) measurements were insufficiently reliable for relative quantification. Albumin (ALB) and transthyretin (TTR) decreased in RNA-seq.

Conclusions

Acute phosphate-salt exposure was associated with reduced HJV expression and exploratory changes in other iron- and heme-related transcripts. These observations do not establish pathway specificity, hepcidin activation, or cellular iron retention.

Introduction

Phosphate balance and iron availability are connected through endocrine and inflammatory processes. Experimental work in mice has linked dietary phosphorus loading to reduced erythropoiesis, low serum iron, and iron retention in tissues [1]. Such systemic observations do not establish how phosphate exposure affects hepatocytes themselves. Defining the hepatic transcriptional response may help distinguish potential cellular effects from changes mediated by the whole-body endocrine environment.

The liver contributes to iron transport and heme handling and is a major site of hepcidin production. Transferrin (TF) transports iron in plasma, whereas hemopexin (HPX) binds heme and supports its

receptor-mediated clearance [2]. Hepatic iron sensing involves transferrin receptor 2 (TFR2) and hemojuvelin (HJV), and matriptase-2, encoded by TMPRSS6, can inhibit hepcidin activation through cleavage of membrane hemojuvelin [3,4]. Because these components have different regulatory functions, their transcript levels cannot be interpreted as interchangeable markers of iron excess or deficiency.

Phosphate-associated transcriptional changes also need to be interpreted in the context of hepatocyte differentiation and function. A recent HepaRG study reported attenuation of the albumin-producing phenotype following phosphate-salt exposure [5]. HNF4α-dependent regulation provides another connection between hepatic identity and iron-related gene expression, including TFR2 [6]. Changes in iron-associated transcripts may therefore accompany a broader alteration in hepatic phenotype rather than a selective iron-sensing response.

Here, we examined iron- and heme-related transcripts in a HepaRG RNA sequencing (RNA-seq) dataset and evaluated selected findings by qPCR. We focused on the phosphate-versus-vehicle contrast and also report measurements that did not reproduce the RNA-seq direction. Our objective was to characterize this transcriptional pattern, not to infer cellular iron accumulation from gene expression alone.

Materials and methods

Cell culture and treatment

HepaRG cells were obtained from KAC Co., Ltd. and maintained in Medium670 at 37°C in a humidified atmosphere with 5% CO2, following the supplier's instructions. No additional differentiation induction was performed. Culture and treatment conditions followed the previously reported HepaRG protocol [5]. The two conditions were vehicle (V) and inorganic phosphate (P). Treatments were applied for 24 h. The final total phosphate concentration in the P condition was 5.0 mM.

A 0.5 M phosphate stock at pH 7.4 was prepared from 0.5 M Na2HPO4 and 0.5 M NaH2PO4 solutions mixed at an 81:19 volume ratio. The complete medium contained 1.12 mM basal phosphate according to the manufacturer; 3.88 mM phosphate was therefore added to obtain the final concentration of 5.0 mM. Added water volumes were matched across conditions. The previously reported medium characterization indicated approximately 1.85 mM calcium, with calculated increases of approximately 7.0 mM sodium and 10.9 mOsm/L from the phosphate salts under the 5.0 mM condition [5]. These values were taken from the previous report and were not re-measured in the present study. Sodium- and osmolality-matched controls, direct osmolality measurements, and particle characterization were not included in that protocol.

RNA-seq used three independent HepaRG cell lots, as in the prior study [5]. The same cell lots and samples were used for qPCR: the three RNA-seq samples corresponded to qPCR cultures 1 to 3, and cultures 4 to 6, where analyzed, were not sequenced. The experimental unit for qPCR was an independent culture experiment, with conditions matched within experiments. Independent HepaRG cell

lots served as biological replicates [5]. Cell viability and ERK activation under these conditions were reported previously [5] and were not re-assessed here.

RNA-seq and expression analysis

The RNA-seq dataset analyzed here contained three vehicle-treated and three phosphate-treated samples after 24 h of treatment. Total RNA was extracted using a Promega RNA extraction kit according to the manufacturer's instructions. Sequencing was outsourced to FUJIFILM Wako Pure Chemical Industries, Ltd., which performed library preparation, sequencing, read processing, alignment, and expression quantification, as described previously [5]. Raw counts and transcripts per million (TPM) were used for the current analysis.

Differential-expression estimates were taken from the original TCC analysis, which used TMM normalization and edgeR. M-values were defined as log2(P/V), so positive M-values in the P versus V comparison indicate higher expression in phosphate-treated samples. In the original analysis, the TCC M-value was used as the log2 fold change (P versus V) and the TCC q-value as the false discovery rate-adjusted value, with $q < 0.05$ regarded as differentially expressed [5, 7]. The count and TPM matrices were checked for agreement with those underlying the original differential-expression results. The principal differential-expression models were not re-fitted; a sensitivity reanalysis is described under Statistical analysis.

The displayed panel comprised TF, HPX, HJV, TMPRSS6, TFR2, ALAD, HMOX1, BLVRA, FTH1, TFRC, and SLC40A1. ALB and TTR were included as hepatic-function comparators. This panel was selected after exploratory examination of the dataset and was not a prospectively specified gene set. Heatmaps used row-standardized log2(TPM + 1) values. Mean TPM ratios were treated as descriptive quantities and distinguished from normalized M-values. HAMP was evaluated separately because of its very low abundance and absence from the differential-expression results table.

Quantitative PCR

RNA was isolated using the ReliaPrep RNA Cell Miniprep System (Promega; Z6012). RNA concentration and purity were assessed with a NanoDrop 2000 spectrophotometer (Thermo Fisher Scientific). One microgram of total RNA was reverse-transcribed using ReverTra Ace qPCR RT Master Mix (TOYOBO; FSQ-201). Amplification used SYBR Green qPCR Master Mix (Thermo Fisher Scientific; A66732) and a QuantStudio 1 Real-Time PCR System (Thermo Fisher Scientific), following the previously reported protocol [5].

The four reference genes were HPRT1, TBP, RPLP0, and 18S rRNA. Relative transcript abundance was normalized to the reference-mix Ct, the arithmetic mean Ct of the four reference genes, which is equivalent to the geometric mean of their relative expression when amplification efficiencies are equal, and calculated using the ΔΔCt approach, consistent with the prior method [5]. Primer sequences and

reference-mix Ct values are provided in Online Resource 1; the assays were reported with reference to the MIQE 2.0 guidelines [8].

For HJV, HPX, HMOX1, TFR2, ALAD, and BLVRA, technical duplicate Ct measurements were averaged before subtraction of the reference-mix Ct. Relative expression was calculated against the matched vehicle sample using the 2^-ΔΔCt approach, which assumes 100% amplification efficiency. For TF, TMPRSS6, and FTH1, relative quantities had been calculated for each technical duplicate. These were combined using their geometric mean and divided by the corresponding vehicle geometric mean. This preserves the log-scale combination of the recorded relative quantities; the underlying quantities were calculated with the same 2^-ΔΔCt procedure and reference-mix normalization.

The primary analysis included all available cultures without excluding culture 4 where its records were available: six cultures for HJV and HPX, four for TF, TMPRSS6, and FTH1, four (cultures 1, 2, 3, and 6) for TFR2, ALAD, and BLVRA, and five for HMOX1. HMOX1 data were available for cultures 1, 2, 3, 5, and 6 only; HMOX1 was therefore analyzed as an available-case analysis. Analyses excluding culture 4 for HJV and HPX were performed as sensitivity analyses, without presuming that its exclusion was technically justified; the Holm family was recomputed for these analyses. For sensitivity analyses without reference normalization (HJV, HPX, HMOX1, TFR2, ALAD, and BLVRA), technical duplicate target Ct values were averaged, and the difference between phosphate-treated and matched vehicle samples was calculated. Ratios were expressed as 2 raised to the negative of this Ct difference, assuming equal RNA input and 100% amplification efficiency. For TF, TMPRSS6, and FTH1, four cultures were available, and their identities were not recorded. TTR, HIF1A, GDF15, and APOA1 were examined descriptively; APOA1 was analyzed from raw Ct values in cultures 1, 2, 3, and 6 and was included as an additional hepatic-function comparator.

HAMP was assessed for quantification reliability before interpretation. Given marked disagreement between some technical duplicates, HAMP fold changes were not used for inference. No assay-specific lower limit of quantification was established from the available records.

Statistical analysis

The principal RNA-seq contrast was P versus V, with significance defined as FDR < 0.05 using the q-values from the original analysis. The nine principal qPCR contrasts were P versus V for the iron- and heme-related genes of the RNA-seq panel that were measured by qPCR: TF, HPX, HJV, TMPRSS6, FTH1, HMOX1, TFR2, ALAD, and BLVRA. Two-sided paired t-tests were performed on ΔCt differences or equivalent log2 relative-quantity contrasts, and Holm correction was applied across these nine tests [9]. This multiplicity definition was chosen for the current exploratory analysis and was not a preregistered analysis plan. TFR2, ALAD, and BLVRA were measured and added after the first six targets had been analyzed; the family was defined by the set of genes measured by qPCR and not by their results. As a secondary sensitivity analysis, Benjamini–Hochberg adjustment of the same nine p-values was added

after the primary results had been obtained; Holm correction remained the primary analysis, and the conclusions are based on it.

qPCR effect estimates are reported as geometric mean fold changes with unadjusted 95% confidence intervals obtained on the log scale. These intervals are not simultaneous intervals and should not be interpreted as equivalent to the Holm-adjusted tests. The main qPCR figure shows matched individual culture values. Technical duplicate wells were not treated as independent observations. Exploratory targets were displayed descriptively. Analyses used Python 3.13.16 with NumPy 2.5.3 and SciPy 1.18.1 [10] (figures were prepared with Matplotlib 3.11.2).

Sensitivity analyses of the RNA-seq data. To assess whether the RNA-seq findings depended on the original TCC analysis, the six-sample (V and P) count matrix was reanalyzed with a limma-voom workflow [11–13]. Genes with low expression were removed using the edgeR filterByExpr criteria (minimum count 10, minimum total count 15, detection in at least three samples), and library sizes were normalized by the trimmed mean of M values (TMM) method [14]. After voom precision weighting, the P effect was estimated with a linear model (~ P) fitted to the six V and P samples, with empirical-Bayes moderation and Benjamini–Hochberg adjustment. The mean–variance trend was estimated by LOWESS. Because each of the three cell lots supplied one V and one P sample, a sensitivity model with lot as a blocking factor (~ lot + P) was also fitted; the unblocked model was kept as the principal voom model because it parallels the original two-group TCC comparison. The workflow was implemented in Python and not in R (NumPy 2.5.3, SciPy 1.18.1, statsmodels 0.15.0, and inmoose 0.9.1, using its limma functions lmFit and squeezeVar). Agreement between qPCR and RNA-seq was summarized by Pearson and Spearman correlations of log2 fold changes for the nine genes quantified by both methods; because n = 9, this comparison is descriptive.

Results

RNA-seq identified lower expression of several iron- and heme-related genes

Phosphate-exposed samples showed lower expression of HJV, TF, HPX, and ALAD (Fig. 1). Their M-values were − 1.459, − 0.831, − 0.623, and − 0.653, respectively, with FDR values of 0.00019, 0.0039, 0.0010, and 0.00020. Mean TPM ratios for P versus V were 0.40 for HJV, 0.62 for TF, 0.72 for HPX, and 0.70 for ALAD. These descriptive ratios were distinct from the normalized effect estimates used in differential-expression testing.

TFR2 and TMPRSS6 also showed lower expression estimates, but their FDR values were 0.052 and 0.075, respectively. HMOX1, BLVRA, and FTH1 showed positive M-values, with FDR values of 0.175, 0.083, and 0.285. TFRC and SLC40A1 did not meet the FDR threshold (FDR 0.739 and 0.097, respectively). Thus, the RNA-seq analysis did not establish a uniform increase in iron-storage or heme-degradation transcripts.

ALB and TTR were also lower in the phosphate group, with FDR values of 0.00057 and 0.011. These changes indicate that the observed pattern extended beyond genes conventionally assigned to iron regulation.

A limma-voom reanalysis supported the RNA-seq findings

In the limma-voom model of the six V and P samples (13,463 genes tested), HJV (log2 fold change − 1.44; FDR 1.7×10^{-4}), TF (− 0.80; 0.0032), HPX (− 0.60; 7.8×10^{-4}), and ALAD (− 0.63; 1.8×10^{-4}) remained below FDR 0.05, as did ALB (1.2×10^{-4}) and TTR (0.010). TFR2 (0.058), TMPRSS6 (0.093), BLVRA (0.079), HMOX1 (0.18), FTH1 (0.11), SLC40A1 (0.13), and TFRC (0.63) did not meet the threshold. The same six of the 13 genes were therefore significant in both analyses, and the direction of the estimates was the same for all 13. A sensitivity model with lot as a blocking factor (~ lot + P) left the estimated log2 fold changes essentially unchanged (correlation across genes 0.99; same direction for all 13 genes) but gave smaller FDR values. The six genes above remained significant (FDR < 1×10^{-5} each), and TFR2 (0.024), TMPRSS6 (0.0033), BLVRA (higher; 0.037), and FTH1 (higher; 0.00046) also fell below 0.05, whereas HMOX1 (0.10), SLC40A1 (0.11), and TFRC (0.65) did not. Only three lots were available, and whether TFR2, TMPRSS6, BLVRA, and FTH1 met the FDR threshold depended on the choice of model (Online Resource 2). For example, the log2 P/V ratio of FTH1 was − 0.04, 1.37, and 1.35 in lots 1 to 3, whereas TFR2, TMPRSS6, and BLVRA changed in the same direction in all three lots. The FTH1 increase was not reproduced by qPCR (see below).

qPCR supported reduced HJV expression with less certain changes in TF, HPX, TMPRSS6, TFR2, and ALAD

HJV expression was lower in all six cultures, with a geometric mean P-to-V ratio of 0.268 (unadjusted 95% CI, 0.157–0.458; Holm-adjusted p = 0.013; Fig. 2 and Table 1). TF, HPX, TMPRSS6, TFR2, and ALAD were also lower in each analyzed culture (Figs. 2 and 3). Their geometric mean ratios were 0.396, 0.516, 0.425, 0.460, and 0.422, respectively, with Holm-adjusted p-values of 0.11 for TF, HPX, TFR2, and ALAD and 0.12 for TMPRSS6. These findings were directionally consistent with RNA-seq but did not reach statistical significance after Holm adjustment. In the secondary Benjamini–Hochberg analysis, adjusted p-values were 0.013 for HJV, 0.033 for TF, HPX, TFR2, and ALAD, and 0.046 for TMPRSS6, but 0.24, 0.55, and 0.74 for BLVRA, FTH1, and HMOX1 (Table 1). Because this procedure controls the false discovery rate rather than the family-wise error rate and was added after the primary results were known, it is reported as a sensitivity analysis, and the conclusions rest on the Holm-adjusted results. The TFR2 estimate agreed in direction with the RNA-seq estimate, which did not meet the FDR threshold in the TCC or ~ P limma-voom analyses (it did in the lot-adjusted model), and the ALAD estimate agreed with its significant RNA-seq decrease.

Table 1
Available-case qPCR estimates for phosphate versus vehicle

Gene	n	Geometric mean ratio	95% CI	Holm p	BH p
TF	4	0.396	0.218–0.718	0.1119	0.0326
HPX	6	0.516	0.316–0.843	0.1119	0.0326
HJV	6	0.268	0.157–0.458	0.0131	0.0131
TMPRSS6	4	0.425	0.210–0.860	0.1229	0.0461
FTH1	4	0.947	0.763–1.177	0.9719	0.5467
HMOX1	5	0.949	0.633–1.425	0.9719	0.7402
TFR2	4	0.460	0.285–0.741	0.1119	0.0326
ALAD	4	0.422	0.235–0.755	0.1119	0.0326
BLVRA	4	0.846	0.616–1.160	0.5712	0.2448

n denotes independent cultures. Confidence intervals are unadjusted. Holm correction covers the nine displayed targets and is the primary analysis; BH p is the Benjamini–Hochberg adjusted p-value for the same nine tests, added as a secondary sensitivity analysis. HMOX1 data were unavailable for culture 4. Cultures analyzed: 1–6 for HJV and HPX; 1, 2, 3, 5, and 6 for HMOX1; four cultures (identities not recorded) for TF, TMPRSS6, and FTH1; cultures 1, 2, 3, and 6 for TFR2, ALAD, and BLVRA. Unadjusted p-values: HJV 0.0015, TF 0.016, HPX 0.018, TMPRSS6 0.031, FTH1 0.49, HMOX1 0.74, TFR2 0.014, ALAD 0.018, and BLVRA 0.19.

FTH1 and HMOX1 qPCR estimates were close to unity: 0.947 (95% CI, 0.763–1.177) and 0.949 (95% CI, 0.633–1.425), respectively. Both had Holm-adjusted p = 0.972. BLVRA, which also had a positive RNA-seq M-value, was likewise not increased (Fig. 3; 0.846; 95% CI, 0.616–1.160; Holm-adjusted p = 0.57). The upward RNA-seq estimates were therefore not reproduced by qPCR. This result does not demonstrate equivalence or exclude changes within the confidence intervals, which are wide for HMOX1.

TTR, HIF1A, GDF15, and APOA1 are presented as exploratory measurements (Online Resource 3; four cultures each, unadjusted for multiplicity). TTR was lower (geometric mean ratio 0.517; 95% CI, 0.334–0.802), HIF1A was similar to vehicle (1.135; 0.860–1.496), GDF15 was higher (1.930; 1.167–3.192), and APOA1 was lower (0.494; 0.359–0.678). APOA1, a hepatic-function comparator added at the qPCR stage, was also lower in the limma-voom analysis (FDR 0.0094).

HAMP measurements did not support reliable relative quantification

Mean HAMP abundance in the RNA-seq data was 0.081 TPM in V and 0.018 TPM in P, with zero values in several samples. HAMP was not represented in the source differential-expression results. These low values were insufficient to support a quantitative inference of downregulation.

Recorded qPCR Ct values in V and P wells ranged from 31.88 to 37.78. Three of 10 technical duplicate pairs with two conventional Ct values differed by more than one cycle. One vehicle pair differed by approximately 4.95 cycles. Accordingly, HAMP was not classified as increased, decreased, or unchanged. Its records are provided in Online Resource 1 for measurement transparency rather than as a relative-expression result.

Sensitivity analyses of culture 4 exclusion and reference normalization

Excluding culture 4 did not reverse the direction of the HJV or HPX findings (Online Resource 4). After exclusion, geometric mean P-to-V ratios were 0.304 for HJV (95% CI, 0.172–0.537; unadjusted p = 0.0044; Holm-adjusted p = 0.039 after recomputing the nine-test family) and 0.571 for HPX (95% CI, 0.329–0.990; unadjusted p = 0.048; Holm-adjusted p = 0.19), compared with 0.268 and 0.516 in the primary analysis. The multiplicity-adjusted conclusions were unchanged after excluding culture 4: HJV remained significant, whereas HPX was not significant in either the six-culture primary analysis (Holm-adjusted p = 0.11) or the five-culture sensitivity analysis. Culture 4 did, however, influence the HPX effect size and unadjusted p-value (ratio 0.516 versus 0.571; unadjusted p = 0.018 versus 0.048). These sensitivity results show how the estimates depend on sample inclusion; they do not establish that the original exclusion was technically justified. The reference-mix Ct was lower in P than in V in all six cultures (mean difference − 0.47 cycles; range − 0.18 to − 0.92 cycles; Online Resource 1), corresponding to an approximately 1.4-fold higher apparent abundance of the reference genes. Without reference normalization, geometric mean P-to-V ratios were 0.372 for HJV (95% CI, 0.243–0.568), 0.715 for HPX (0.471–1.086), 1.236 for HMOX1 (0.815–1.874), 0.595 for TFR2 (0.421–0.841), 0.545 for ALAD (0.351–0.847), and 1.094 for BLVRA (0.866–1.382); the HPX estimate in particular therefore depended on the reference normalization. The TFR2 and ALAD decreases persisted without reference normalization (unadjusted p = 0.017 and 0.022). The RNA-seq data showed the same tendency: mean TPM of HPRT1 and TBP was higher in P than in V (ratios 1.29 and 1.28), whereas RPLP0 changed little (1.08).

Concordance between qPCR and RNA-seq. Across the nine genes quantified by both methods, the log2 ratios from qPCR correlated closely with the limma-voom log2 fold changes (Pearson r = 0.97; Spearman ρ = 0.87; n = 9), but the qPCR values were lower by a mean of 0.56 log2 units (SD 0.19; approximately 1.5-fold), similar in size to the 0.47-cycle shift in the reference-mix Ct. For HJV, HPX, HMOX1, TFR2, ALAD, and BLVRA, for which Ct values permitted analysis without reference normalization, the mean absolute difference from the RNA-seq log2 fold change was 0.12 without reference normalization and 0.47 with it. These descriptive comparisons (nine genes; RNA-seq estimates are themselves relative to library composition) showed directional concordance between methods but do not constitute independent validation, because cultures 1 to 3 were shared. The qPCR estimates were lower than the RNA-seq estimates as a group, and closer agreement without reference normalization does not establish that the unnormalized estimates are more accurate.

Discussion

This study describes a phosphate-associated transcriptional pattern in HepaRG cells involving HJV and several genes related to iron transport and heme handling. HJV provided the clearest agreement between RNA-seq and multiplicity-adjusted qPCR. TF, HPX, TMPRSS6, TFR2, and ALAD showed consistent downward qPCR estimates, but uncertainty remained after correction across the nine principal comparisons. The findings therefore support a focused description of gene expression rather than a demonstrated mechanism of iron retention. A limma-voom reanalysis supported the RNA-seq results, and the direction of change across genes agreed between RNA-seq and qPCR. In the lot-adjusted sensitivity model, FTH1 (higher in RNA-seq, but not consistently across lots) was the clearest disagreement with qPCR, which we could not resolve. The magnitude of the qPCR decreases, however, depended on reference normalization. The primary reference-normalized analysis estimated an HJV P-to-V ratio of 0.268. A sensitivity analysis without reference normalization yielded a ratio of 0.372, retaining the direction of the change under a different set of assumptions.

HJV is relevant to hepcidin regulation as a BMP co-receptor, and HJV mutations cause juvenile hemochromatosis [15, 16], but reduced HJV expression cannot by itself establish the direction of hepcidin output. TMPRSS6 acts at a different regulatory step and can oppose hepcidin activation [4]. Concurrent decreases in their transcripts, together with the lower TFR2 level, do not identify which effect predominates. Moreover, HAMP could not be reliably quantified, and neither hepcidin protein nor ferroportin protein was assessed. A possible sequence of phosphate exposure, hepcidin induction, and impaired iron release remains untested in this dataset. Inflammatory induction of hepcidin is mediated largely by IL-6 [17], and IL6 expression was not robustly induced by phosphate in the previous study [5]; an inflammatory route is therefore not the most obvious explanation for the HJV change, although this was not tested directly.

The TF and HPX findings provide a rationale for measuring their extracellular protein concentrations. The qPCR estimates were not negligible: the geometric mean ratios were approximately 0.40 and 0.52, respectively. Nevertheless, the adjusted tests and small sample sizes require cautious interpretation. Protein measurements would address a distinct question rather than retrospectively validate a nonsignificant qPCR test. Agreement between transcript and extracellular protein results would strengthen evidence for an effect extending beyond transcription, whereas discordance would constrain that interpretation. Culture-supernatant concentrations would still need to be interpreted in relation to medium composition, cell abundance, and possible uptake or degradation.

The heme-related findings also require separation of transcript abundance from metabolic activity. ALAD was reduced in RNA-seq, and its qPCR estimate was also lower (ratio 0.42; Holm-adjusted $p = 0.11$), although this did not meet the adjusted threshold. However, neither ALAD enzyme activity nor heme synthesis was measured. HMOX1 did not show qPCR induction, and its RNA-seq estimate was not FDR-significant. BLVRA likewise showed no clear qPCR change (ratio 0.85). These observations do not support a claim of coordinated enhancement of heme degradation.

A broader change in hepatic phenotype is an important alternative explanation. ALB and TTR decreased in the RNA-seq analysis, and TTR and APOA1 showed lower qPCR estimates in the exploratory measurements (Online Resource 3), and APOA1 was also lower in the limma-voom analysis. Prior HepaRG work has associated phosphate-salt exposure with attenuation of the albumin-producing phenotype [5]. The experimental connection between HNF4α and hepatic iron-related genes [6] further supports consideration of hepatic identity when interpreting these results. Because TFR2 is regulated by HNF4α in mouse liver [6], the lower TFR2 estimate (ratio 0.46) cannot be separated from a general decrease in hepatocyte-specific gene expression, which the similar reduction of APOA1 (0.49) also suggests. The present study does not distinguish selective regulation of iron-associated genes from a wider change in hepatocyte function. GDF15, a stress-responsive secreted factor, was higher in the exploratory measurements (ratio 1.93; unadjusted $p = 0.025$), which may indicate a cellular stress response but was not examined further.

The clinical implications remain indirect. Dietary phosphorus can affect iron homeostasis through systemic pathways [1], whereas the present work examines a cultured hepatic model. It does not measure erythropoietic iron availability, circulating hepcidin, or patient outcomes. A hepatic transcriptional response in this model should therefore not be equated with functional iron deficiency in patients receiving dialysis. In CKD, elevated hepcidin contributes to functional iron deficiency [18]; whether phosphate exposure alters hepatic hepcidin regulation directly remains to be determined.

Several limitations affect interpretation. The sample sizes were small, limiting precision and assessment of distributional assumptions. With only three lots, whether several genes (TFR2, TMPRSS6, BLVRA, and FTH1) met the FDR threshold in the RNA-seq analysis depended on the choice of model. HepaRG cells derive from a single donor, so independent cell lots do not represent biological replication across individuals. Target selection followed exploratory RNA-seq analysis, so the qPCR findings are not a fully independent, prospectively specified confirmatory test. Because RNA-seq and qPCR used the same material for cultures 1 to 3, the qPCR results in those cultures are a second measurement of the same samples and not independent replication; only cultures 4 to 6, where analyzed (for TFR2, ALAD, and BLVRA, only culture 6), are independent of the RNA-seq samples. Some qPCR analyses relied on recorded relative quantities rather than raw Ct values, and the reference-gene aggregation and efficiency assumptions require complete reporting. The reference-mix Ct was consistently lower in P than in V (mean − 0.47 cycles), so normalization to reference genes whose abundance may itself respond to phosphate [19] could have contributed to the apparent decreases, particularly for HPX. All six available cultures were retained for HJV and HPX, but HMOX1 records for culture 4 were unavailable. Differing sample availability across genes limits comparison. TFR2, ALAD, and BLVRA were measured in four cultures (1, 2, 3, and 6), and their correspondence with the four cultures used for TF, TMPRSS6, and FTH1 was not recorded. The Holm family of nine tests was defined by the genes measured, and three of the nine targets were added after the first six had been analyzed; adjusted p-values depend on this definition, although HJV remained significant and the other targets remained nonsignificant for families of six to nine tests. Under Benjamini–Hochberg adjustment, six of the nine targets (HJV, TF, HPX, TMPRSS6, TFR2, and ALAD) had adjusted $p < 0.05$, compared with one under Holm correction, so the number of

targets classified as changed depended on the multiplicity procedure. The low and inconsistent HAMP signal limited evaluation of hepcidin regulation. Finally, protein abundance (including that of HJV), intracellular iron, heme content, and iron export were not measured. The acute 24 h exposure to 5.0 mM total phosphate is supraphysiological and does not reproduce chronic CKD. HepaRG cells retain many hepatocyte-like properties and resemble primary hepatocytes more closely than HepG2 cells [20, 21], but remain a single-donor model. As in the prior protocol [5], sodium- and osmolality-matched controls and characterization of calcium-phosphate or protein-mineral particles were not included. The observed effects therefore cannot be attributed specifically to dissolved phosphate.

Conclusion

Acute phosphate-salt exposure was associated with reduced HJV expression in HepaRG cells and with exploratory changes in additional iron- and heme-related transcripts. HJV, TF, and HPX remain candidates for protein-level investigation, although only HJV met the multiplicity-adjusted significance threshold in qPCR. The current data support a transcriptional study and do not establish hepcidin activation or hepatic iron trapping.

Abbreviations

CI
confidence interval
Ct
quantification cycle
FDR
false discovery rate
qPCR
quantitative polymerase chain reaction
RNA-seq
RNA sequencing
TPM
transcripts per million
TCC
tag count comparison
TMM
trimmed mean of M-values
V
vehicle
P
phosphate

Declarations

Consent to participate:

Not applicable to the reported cell-line experiments.

Consent for publication:

Not applicable; no individual patient data are reported.

Ethics approval:

Not applicable. This study used a commercially obtained human cell line (HepaRG; KAC Co., Ltd.) and did not involve human participants or animals.

Competing interests:

The authors declare no competing interests.

Prior use of data:

The RNA-seq dataset and culture protocol were previously reported in [5], which examined albumin, HNF4A, and IL6 expression, albumin secretion, cell viability, and ERK phosphorylation in phosphate-treated HepaRG cells. The present study addresses a distinct question: the response of iron- and heme-related transcripts to phosphate exposure.

Funding:

This research was supported by the Japan Society for the Promotion of Science, Grant-in-Aid for Scientific Research (C) (24K10046 to T.H. and 26K11437 to Y.H.).

Author Contribution

TH and YH conceived and designed the study. TH, YK, YY, TS, YM, and YH contributed to experiments, data analysis, or interpretation of data. TH, YM, and YH drafted the manuscript. All authors read and approved the final manuscript.

Acknowledgments:

Not applicable.

Data Availability

The RNA-seq data analyzed here are those deposited in the DDBJ Sequence Read Archive for the previous report [Honda et al., 2026] (BioProject PRJDB42291; BioSample SAMD01917852–SAMD01917855; Experiment DRX1026069–DRX1026080; Run DRR1050402–DRR1050413). Only the vehicle- and phosphate-treated samples (six of the 12 deposited samples) were analyzed in the present study. The count and TPM matrices, the sample-to-lot table, qPCR data, and analysis scripts (including the Python limma-voom code) are available from the corresponding author on reasonable request.

References

1. Park MY, Agoro R, Jankauskas SS, Le Henaff C, Sitara D (2024) Phosphorus-independent role of FGF23 in erythropoiesis and iron homeostasis. PLoS One 19:e0315228. https://doi.org/10.1371/journal.pone.0315228
2. Hvidberg V, Maniecki MB, Jacobsen C, Højrup P, Møller HJ, Moestrup SK (2005) Identification of the receptor scavenging hemopexin-heme complexes. Blood 106:2572–2579. https://doi.org/10.1182/blood-2005-03-1185
3. Rapisarda C, Puppi J, Hughes RD et al (2010) Transferrin receptor 2 is crucial for iron sensing in human hepatocytes. Am J Physiol Gastrointest Liver Physiol 299:G778–G783. https://doi.org/10.1152/ajpgi.00157.2010
4. Silvestri L, Pagani A, Nai A, De Domenico I, Kaplan J, Camaschella C (2008) The serine protease matriptase-2 (TMPRSS6) inhibits hepcidin activation by cleaving membrane hemojuvelin. Cell Metab 8:502–511. https://doi.org/10.1016/j.cmet.2008.09.012
5. Honda T, Sakaguchi T, Kondo Y, Yabune Y, Motomiya Y, Higashimoto Y (2026) Acute phosphate-salt exposure is associated with attenuation of the albumin-producing phenotype, HNF4A down-regulation, and ERK activation in HepaRG cells. BMC Nephrol. https://doi.org/10.1186/s12882-026-05334-w
6. Matsuo S, Ogawa M, Muckenthaler MU et al (2015) Hepatocyte nuclear factor 4α controls iron metabolism and regulates transferrin receptor 2 in mouse liver. J Biol Chem 290:30855–30865. https://doi.org/10.1074/jbc.M115.694414
7. Sun J, Nishiyama T, Shimizu K, Kadota K (2013) TCC: an R package for comparing tag count data with robust normalization strategies. BMC Bioinformatics 14:219. https://doi.org/10.1186/1471-2105-14-219
8. Bustin SA, Ruijter JM, van den Hoff MJB et al (2025) MIQE 2.0: Revision of the Minimum Information for Publication of Quantitative Real-Time PCR Experiments Guidelines. Clin Chem 71:634–651. https://doi.org/10.1093/clinchem/hvaf043
9. Holm S (1979) A simple sequentially rejective multiple test procedure. Scand J Stat 6:65–70
10. Virtanen P, Gommers R, Oliphant TE et al (2020) SciPy 1.0: fundamental algorithms for scientific computing in Python. Nat Methods 17:261–272. https://doi.org/10.1038/s41592-019-0686-2

11. Robinson MD, McCarthy DJ, Smyth GK (2010) edgeR: a Bioconductor package for differential expression analysis of digital gene expression data. Bioinformatics 26:139–140. https://doi.org/10.1093/bioinformatics/btp616
12. Law CW, Chen Y, Shi W, Smyth GK (2014) voom: precision weights unlock linear model analysis tools for RNA-seq read counts. Genome Biol 15:R29. https://doi.org/10.1186/gb-2014-15-2-r29
13. Ritchie ME, Phipson B, Wu D et al (2015) limma powers differential expression analyses for RNA-sequencing and microarray studies. Nucleic Acids Res 43:e47. https://doi.org/10.1093/nar/gkv007
14. Robinson MD, Oshlack A (2010) A scaling normalization method for differential expression analysis of RNA-seq data. Genome Biol 11:R25. https://doi.org/10.1186/gb-2010-11-3-r25
15. Babitt JL, Huang FW, Wrighting DM et al (2006) Bone morphogenetic protein signaling by hemojuvelin regulates hepcidin expression. Nat Genet 38:531–539. https://doi.org/10.1038/ng1777
16. Papanikolaou G, Samuels ME, Ludwig EH et al (2004) Mutations in HFE2 cause iron overload in chromosome 1q-linked juvenile hemochromatosis. Nat Genet 36:77–82. https://doi.org/10.1038/ng1274
17. Nemeth E, Rivera S, Gabayan V et al (2004) IL-6 mediates hypoferremia of inflammation by inducing the synthesis of the iron regulatory hormone hepcidin. J Clin Invest 113:1271–1276. https://doi.org/10.1172/JCI20945
18. Ganz T, Nemeth E (2016) Iron balance and the role of hepcidin in chronic kidney disease. Semin Nephrol 36:87–93. https://doi.org/10.1016/j.semnephrol.2016.02.001
19. Vandesompele J, De Preter K, Pattyn F et al (2002) Accurate normalization of real-time quantitative RT-PCR data by geometric averaging of multiple internal control genes. Genome Biol 3:research0034. https://doi.org/10.1186/gb-2002-3-7-research0034
20. Gripon P, Rumin S, Urban S et al (2002) Infection of a human hepatoma cell line by hepatitis B virus. Proc Natl Acad Sci USA 99:15655–15660. https://doi.org/10.1073/pnas.232137699
21. Hart SN, Li Y, Nakamoto K et al (2010) A comparison of whole genome gene expression profiles of HepaRG cells and HepG2 cells to primary human hepatocytes and human liver tissues. Drug Metab Dispos 38:988–994. https://doi.org/10.1124/dmd.109.031831

Figures

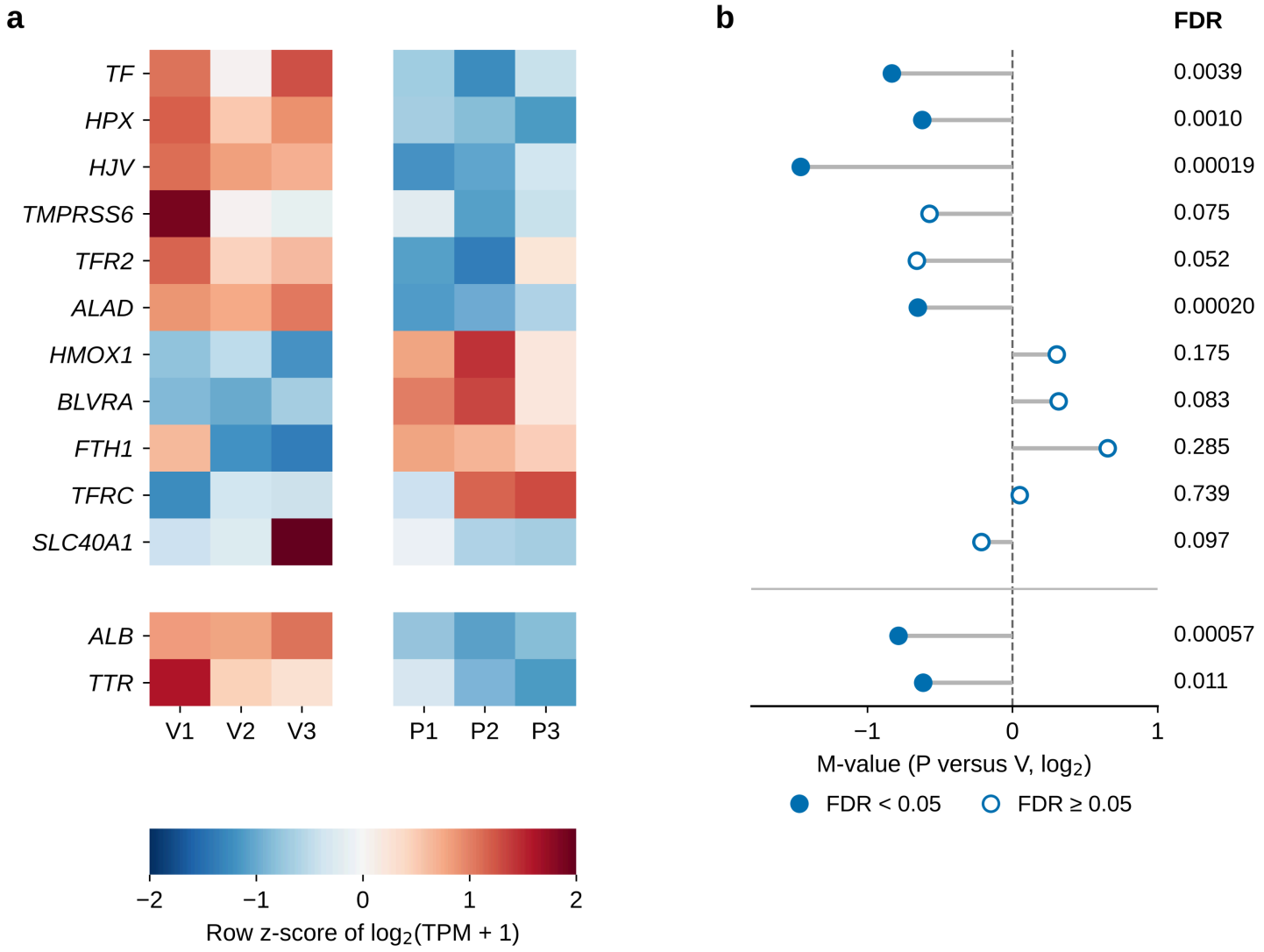


Figure 1

RNA-seq analysis of iron- and heme-related genes. a Heatmap of individual samples. b TCC M-values (P versus V); filled circles indicate FDR < 0.05. Three samples per condition; phosphate versus vehicle. Heatmap values are row-standardized log2(TPM + 1); differential-expression estimates and FDR derive from the existing TCC analysis. ALB and TTR are hepatic phenotype comparators

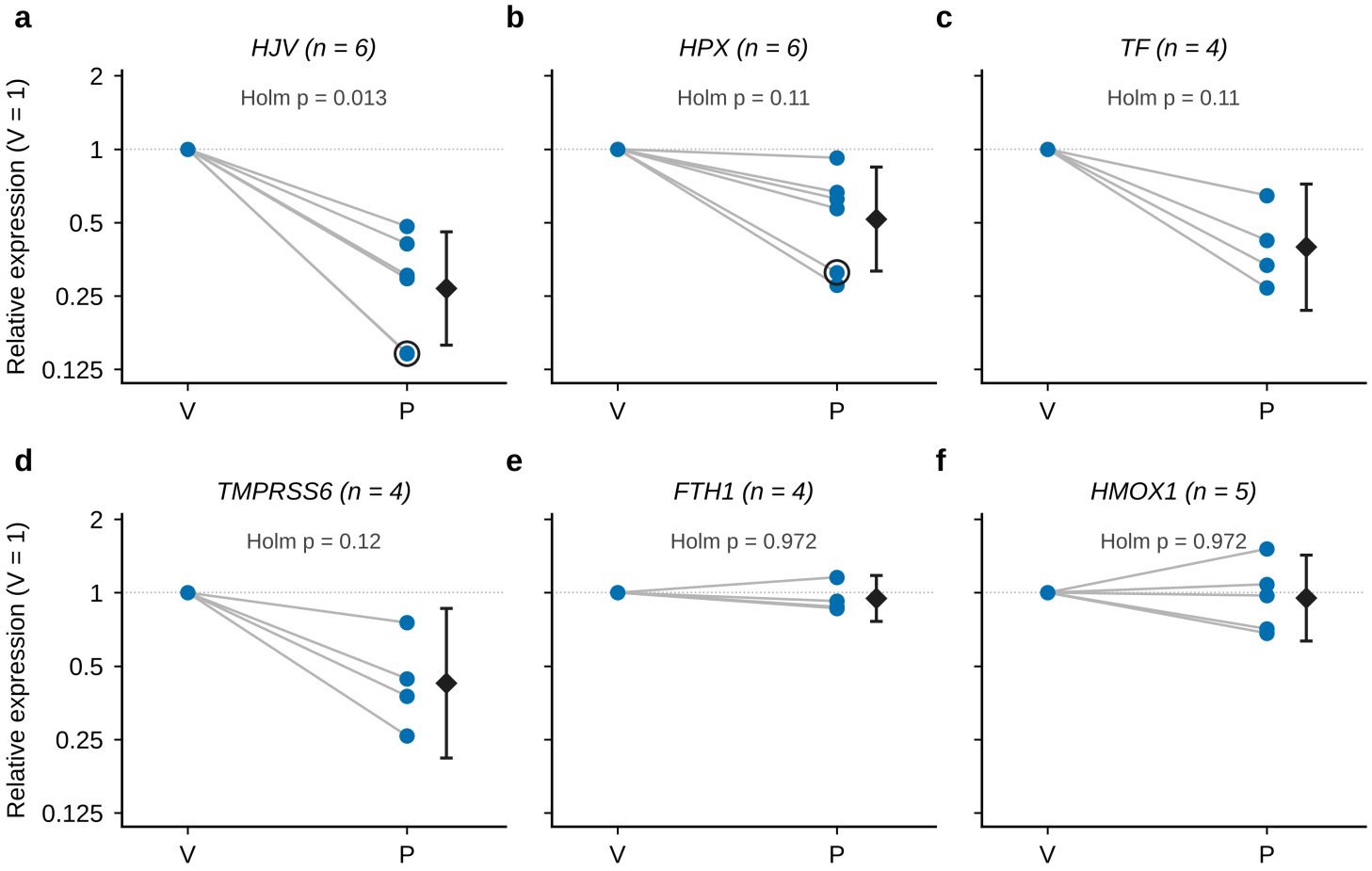


Figure 2

Available-case qPCR for phosphate versus vehicle. Gray lines join matched cultures; black diamonds and bars show the geometric mean with unadjusted 95% confidence intervals; the circled point marks culture 4 (HJV and HPX). Technical duplicates were combined before analysis. HJV and HPX include six cultures; TF, TMPRSS6 and FTH1 include four (identities not recorded); HMOX1 includes five available cultures. Displayed p-values use paired log-scale tests and Holm correction across the nine targets of Figs. 2 and 3

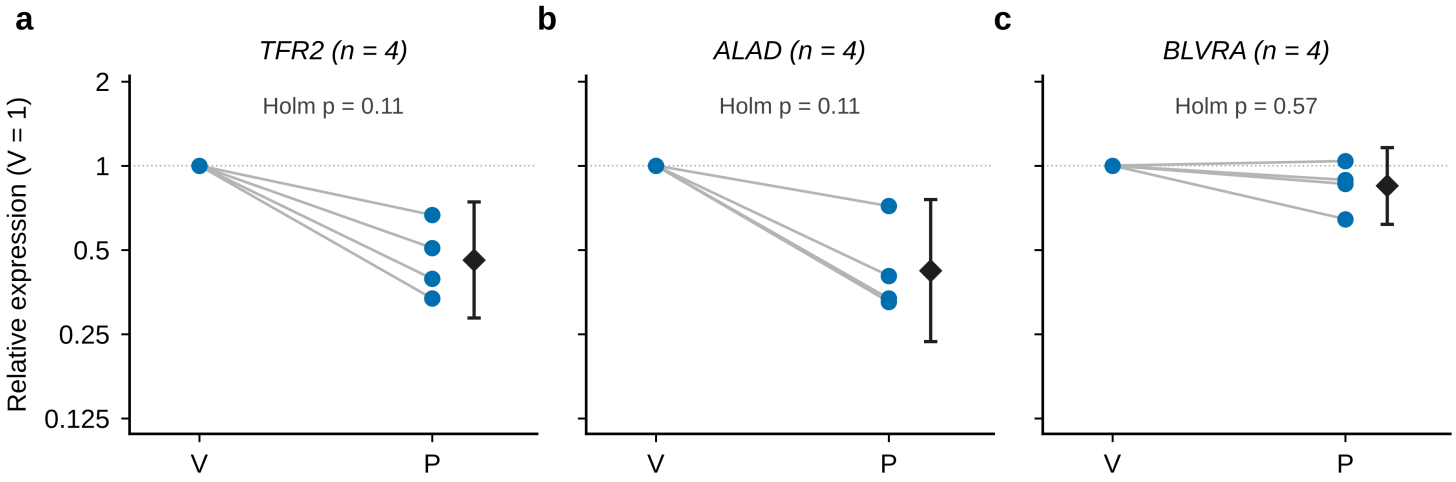


Figure 3

Available-case qPCR for phosphate versus vehicle: TFR2, ALAD, and BLVRA. Gray lines join matched cultures (cultures 1, 2, 3, and 6); black diamonds and bars show the geometric mean with unadjusted 95% confidence intervals. Technical duplicates were combined before analysis. Displayed p-values use paired log-scale tests and Holm correction across the nine targets of Figs. 2 and 3

Supplementary Files

This is a list of supplementary files associated with this preprint. Click to download.

- OnlineResources14.pdf